Pergamon

Int. J. Heat Mass Transfer. Vol. 38, No. 14, pp. 2667–2675, 1995

0017–9310/95 $9.50+0.00

0017–9310(95)00015–1

Numerical analysis of higher order harmonics in the response of a mass transfer probe

ZAI-SHA MAO

Institute of Chemical Metallurgy, Academia Sinica, Beijing 100080, China

(*Received* 24 *August* 1994)

Abstract—The frequency response of a mass transfer probe is investigated by numerical methods in view of the nonlinear interaction of wall shear with the concentration boundary layer at the electrochemical probe. When the fluctuating component of shear is strong, the high order harmonics in the transient mass transfer coefficient is not negligible. This casts doubt on the accuracy of power spectrum data of wall shear stress in high frequency range. Besides, the longitudinal diffusion term plays a noticeable role when the dimensionless length of the electrode is small and the frequency is high. Attention should be paid to the very poor frequency response of a double probe as it is used for the wall shear oscillating around zero.

1. INTRODUCTION

The problem of frequency response of a heat or mass transfer probe has been the subject of numerous studies in the past. Among those investigations both numerical analysis of simplified equations as well as experimental measurements have been reported as by Fortuna and Hanratty [1], Mao and Hanratty [2] and Ambari *et al.* [3].

As for theoretical analysis, the full two-dimensional (2D) convective diffusion equation is simplified in a typical approach using linearization, first by omitting the longitudinal diffusion and limiting the domain of solution to the length of the probe so that diffusion from the regions upstream and downstream of the probe is not accounted for, and then neglecting all the harmonics in the fluctuation of the mass transfer coefficient above the first. Those simplifying assumptions limit the range of application of results. Mao and Hanratty [4] recently extended the solution domain to include the region upstream and downstream of the electrode in an attempt to invert the mass probe output, but still ignored the longitudinal diffusion term. It is desired to investigate the validity of those approximations, and in particular the importance of higher order harmonics to the measurement of wall shear stress.

In this study, direct numerical solution of the full convective diffusion equation in an extended domain is compared with the simplified quasi-steady state analysis to shed light on the validity of the above mentioned simplifications. The attenuation and phase lag of the higher harmonics in the response of a mass transfer probe is examined. In addition, the numerical method was used to study a double probe for oscillating wall shear stress to illustrate the due caution in dealing with the measurement of higher harmonic components. Numerical simulation of the frequency response of a transfer probe is recommended as an indispensable step in designing a probe before conducting experiments.

2. NUMERICAL SIMULATION OF A MASS TRANSFER PROBE

The convective diffusion equation models the transfer of heat and/or mass from the surface of the probe. The mass transfer probe for measurement of wall shear stress and turbulence is usually very small in size, typically $L = 0.05$ to 0.1 mm in the flow direction, made of nickel or platinum foil and imbedded flush in the wall. If a double probe is to be used (Fig. 1), another thin foil of the same size is imbedded next to the first foil with a much thinner electrical insulation layer separating two electrodes. The lateral dimension of the electrode is large enough to allow the flow to be viewed as 2D and parallel with a constant velocity gradient in the flow direction. The general governing equation of mass transfer is

$$\frac{\partial C}{\partial t}+u\frac{\partial C}{\partial x}+v\frac{\partial C}{\partial y}=D\left(\frac{\partial^2 C}{\partial x^2}+\frac{\partial^2 C}{\partial y^2}\right).$$

Since those systems chosen for the wall shear stress

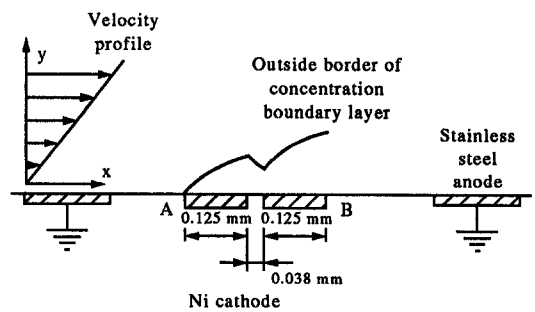

Fig. 1. Sketch of an electrochemical probe.

NOMENCLATURE

A	factor of attenuation of first harmonic of output signal for wall velocity gradient
C	dimensionless concentration
C_{B0}	bulk concentration [mol m^{-3}]
D	diffusivity for mass transfer [m^2 s^{-1}]
f	frequency [s^{-1}]
f^+	dimensionless frequency defined by equation (19)
k	mass transfer coefficient [mol m^{-2} s^{-1}]
L	electrode length in flow direction [m]
L^*	dimensionless electrode length defined by equation (16)
n	harmonic order
R	magnitude ratio of first harmonic to the time average
S	velocity gradient at solid wall [s^{-1}]
t	time [s]
u	velocity component in x-direction [m s^{-1}]
v	velocity component in y-direction [m s^{-1}]
x	longitudinal coordinate [m]
y	transverse coordinate [m]
y^*	dimensionless distance in transverse direction.

Greek symbols

ϕ	phase lag [degree]
ψ	ratio of magnitude response defined by equation (20)
ω	angular frequency [s^{-1}]
ω^+	dimensionless angular frequency defined by equation (9)
ω^*	dimensionless angular frequency defined by equation (15).

Subscripts

i	index of harmonic order
w	wall.

measurement are of high Schmidt number, the concentration boundary layer is very thin and the velocity within the boundary layer can be approximated by $u = Sy$, from which it follows that $v \propto y^2$ for incompressible flow. However, the range of y is restricted by the very small boundary layer thickness and it is readily shown by order of magnitude arguments that the term $v(\partial C/\partial y)$ is negligible. Thus, the analysis starts from

$$\frac{\partial C}{\partial t} + Sy\frac{\partial C}{\partial x} = D\left(\frac{\partial^2 C}{\partial x^2} + \frac{\partial^2 C}{\partial y^2}\right). \tag{1}$$

There exists some misunderstanding on the nature of equation (1). When the electrochemical probe is used in investigating the turbulent nature of fluid flow, it is a popular practice to use

$$k = 0.807\left(\frac{SD^2}{L}\right)^{1/3} \tag{2}$$

which is the solution of the simplified steady state version of equation (1):

$$S_0 y\frac{\partial C_0}{\partial x} = D\frac{\partial^2 C_0}{\partial y^2} \tag{3}$$

without longitudinal diffusion term and subject to constant wall shear [5] to convert the probe output to fluctuating wall shear stress, $S(t)$. Power spectrum of wall shear stress up to 100 Hz is often reported in the literature (for example, Souhar and Cognet [6], Kashinsky [7]). But the accuracy of data at such high frequency is questionable. In fact, the interaction of concentration field with velocity gradient represented by the term $Sy(\partial C/\partial x)$ induces serious limitation on application of equation (2) and generates an infinite series of high order harmonics in the probe output.

It can be shown that, due to this nonlinearity of equation (1), higher harmonics will result even when $S(t)$ consists of a nonzero average and a simple harmonic component only. Suppose the velocity gradient $S(t)$ and the concentration $C(x, y, t)$ take the forms of

$$S(t) = S_0 + \sum_{n=1}^{\infty} S_n \exp(in\omega t) \tag{4}$$

$$C(x, y, t) = C_0(x, y) + \sum_{n=1}^{\infty} C_n(x, y) \exp(in\omega t) \tag{5}$$

then the average component $C_0(x, y)$ is governed by

$$S_0 y\frac{\partial C_0}{\partial x} = D\left(\frac{\partial^2 C_0}{\partial x^2} + \frac{\partial^2 C_0}{\partial y^2}\right) \tag{6}$$

which is the steady state version of the convective diffusion equation under the condition of parallel flow with a constant velocity gradient S_0. All the higher

order harmonic components are involved with lower order ones of $C(x, y, t)$ and $S(t)$:

$$\begin{cases} i\omega C_1(x,y) + S_0 y \dfrac{\partial C_1}{\partial x} = D\left(\dfrac{\partial^2 C_1}{\partial x^2} + \dfrac{\partial^2 C_1}{\partial y^2}\right) - yS_1 \dfrac{\partial C_0}{\partial x} & (7a) \\ 2i\omega C_2(x,y) + S_0 y \dfrac{\partial C_2}{\partial x} = D\left(\dfrac{\partial^2 C_2}{\partial x^2} + \dfrac{\partial^2 C_2}{\partial y^2}\right) - y\left(S_1 \dfrac{\partial C_1}{\partial x} + S_2 \dfrac{\partial C_0}{\partial x}\right) & (7b) \\ \cdots \\ in\omega C_n(x,y) + S_0 y \dfrac{\partial C_n}{\partial x} = D\left(\dfrac{\partial^2 C_n}{\partial x^2} + \dfrac{\partial^2 C_n}{\partial y^2}\right) - y \sum_{k=1}^{n} S_k \dfrac{\partial C_{n-k}}{\partial x}. & (7c) \end{cases}$$

The boundary conditions for the harmonic $C_1, \ldots, C_n, \ldots$ are easy to define. In principle, we can solve for all C_n successively. The mass transfer coefficient is then

$$k(t) = \frac{1}{L}\int_0^L D \frac{\partial C(x,y,t)}{\partial y}\bigg|_w \mathrm{d}x = k_0 + \sum_{n=1}^{\infty} k_n \exp(in\omega t) \tag{8}$$

where the component k_n is dependent on first $n+1$ components of $S(t)$: $S_0, S_1, \ldots$, and S_n. The subscript w in equation (8) indicates evaluating the derivatives at the electrode surface, $y = 0$.

In particular, even if there exists only one harmonic S_1 in the input $S(t)$, there results an infinite series of harmonics both in $C(x, y, t)$ and in the output mass transfer coefficient $k(t)$. Fortuna and Hanratty [1], Mao and Hanratty [2] and Ambari *et al.* [3] simplified the problem by setting all the higher harmonics of $C(x, y, t)$ to be zero and took equation (7a) as the dynamic system simulating the mass transfer process. When the ratio of S_1/S_0 becomes large, this assumption is expected to be in error.

To analytically solve the infinite set of equation (7) is impractical. Under the linearization convention, Mao and Hanratty [2] have shown that equation (7a) depends on a single parameter, the dimensionless frequency

$$\omega^+ = 2\pi f\left(\frac{L^2}{S^2 D}\right)^{1/3}. \tag{9}$$

However, when $S(t) = S_0 + S_1 \exp(i\omega t)$ and the higher harmonics in C are not to be neglected, equation (1) may be put in the dimensionless form,

$$\frac{\partial C}{\partial t^*} + y^* \frac{\partial C}{\partial x^*} + R\exp\left(i\frac{\omega}{S_0}t^*\right) y^* \frac{\partial C}{\partial x^*} = \frac{\partial^2 C}{\partial x^{*2}} + \frac{\partial^2 C}{\partial y^{*2}} \tag{10}$$

where the dimensionless variables are

$$t^* = S_0 t \tag{11}$$

$$x^* = x\sqrt{(S_0/D)} \tag{12}$$

$$y^* = y\sqrt{(S_0/D)}. \tag{13}$$

Thus it is seen that the solution is controlled by the following three parameters:

$$R = S_1/S_0 \tag{14}$$

$$\omega^* = \omega/S_0 \tag{15}$$

$$L^* = L\sqrt{(S_0/D)} \tag{16}$$

the last one resulting from the boundary condition.

It is possible to solve the full convective diffusion equation (10) by a direct numerical method without resorting to simplifying assumptions. For this purpose, a rectangular domain of flow field is chosen instead of a semi-infinite plane. One boundary is the solid wall and the probe surface, and the other three are located far enough from the mass transfer probe, so that the boundary condition there, $C = 1$, can be used, where the dimensionless concentration C is normalized by C_{B0}. The electrode length used for simulation ranges from 0.07 to 0.24 mm and is centered in a 0.03 m long wall. The computational domain extends 2 mm from the wall in the y direction. For a typical ferri/ferrocyanide system, the thickness of concentration boundary layer is about 0.01 mm only.

Numerical solution of the convective diffusion equation in a rectangular domain is rather easy with the control volume formulation discussed in a book by Patankar [8]. UPDS (Upstream Power-law Differencing Scheme) was chosen to discretize the differential equation. More meshes were distributed along the electrode and near the wall, with widely spaced grid lines in the areas far from the probe. The proper mesh size was determined by trial computations of steady state convective diffusion with gradually decreasing cell size, until little change occurred in the resulting mass transfer coefficients. The time interval was chosen small enough so that no additional change of the concentration field occurs as time interval is further reduced. A typical mesh net consisted of 40–50 cells in flow direction and 25 across the flow. Time step was usually about one thousandth of the characteristic time scale: the period of oscillation or other appropriate time scale. Computation was mostly done on the dimensional formulation. The velocity gradient in the x direction was assumed constant for each time instant.

To check the ability of the numerical scheme, steady state mass transfer under constant wall shear was solved and the results were compared with the analytical quasi-steady solution, equation (2). Figure 2 shows that the results of $k(t)$ from the numerical cal-

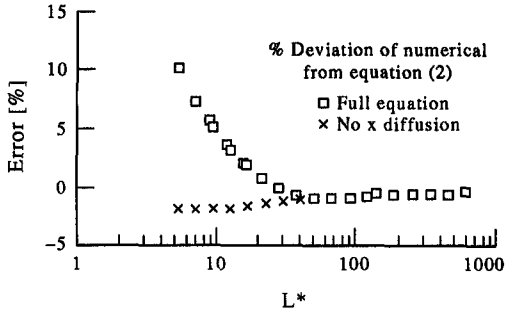

Fig. 2. Comparison of direct numerical simulation with the quasi-steady state solution, equation (2). Longitudinal diffusion term becomes significant when L^* is less than 30.

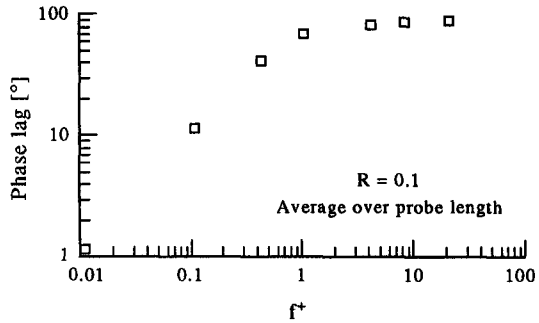

Fig. 3. Phase lag of the first harmonic of average $k(t)$ behind the fluctuation of $S(t)$.

culation for cases with different values of velocity gradient agree very well with equation (2), although there is a small difference. More results were presented by Mao [9] to reveal the relation of the difference to the values of L^*. When $L^* > 30$, the difference between the numerical simulation and equation (2) is negligible, but the longitudinal diffusion omitted in equation (3) creates pronounced deviation from the numerical simulation of the full mass transfer equation when L^* is small. However, small size electrodes are sometime preferred in order to improve the frequency response, and in this case caution is advised for adopting simple and analytical equation (2). Moreover, the transient process of switching on a mass probe was also simulated and the decay of the mass transfer coefficient from the present numerical simulation was in close agreement with the experimental measurements of transient $k(t)$ [9].

3. HIGH ORDER HARMONICS IN THE RESPONSE TO SHEAR WITH A SIMPLE HARMONIC

Numerical computations were carried out for the case of simple harmonic of small amplitude ($R = 0.1$) superimposed on a constant time-average wall shear as depicted by

$$S = S_0(1 + R\sin(2\pi f t)). \tag{17}$$

The attenuation and phase lag of the first harmonic of the mass transfer coefficient $k(t)$ were evaluated by using Fourier analysis for a series of cases. In the limit as $f \to 0$, the pseudo-steady state assumption becomes precise and the fluctuating component k_1 of $k(t)$ can be derived from equation (2). The amplitude of first harmonic is dependent on the strength of the harmonic component in S:

$$1 + \frac{k_1}{k_0} = (1+R)^{1/3} \tag{18}$$

and the phase lag for the first harmonic will approach zero. But as f increases, the phase lag of $k(t)$ behind $S(t)$ and attenuation of the fluctuation in $k(t)$ become evident. The phase lag, ϕ, of the average mass transfer coefficient from the numerical simulation is presented in Fig. 3, where the dimensionless frequency is defined as

$$f^+ = f\left(\frac{L^2}{S_0^2 D}\right)^{1/3}. \tag{19}$$

The asymptotic value is $\pi/2$ for the average phase lag. Figure 4 presents the results of amplitude ratio from numerical simulations, showing that the asymptotic slope of the curve for the amplitude ratio vs f^+ approaches -1.0. Mizushina *et al.* [10] found experimentally that the average Sherwood number under constant wall concentration displayed that the phase lag of first harmonic approached $\pi/2$ and k_1/k_0 became -0.95 as f was high. From the results of linearization it is noted that for the space-averaged $k(t)$ the asymptotic values were $\pi/2$ and about -0.91, respectively [2]. Present results agree well with the values in the above-mentioned literature.

Those average values from the numerical simulations coincide well with the phase lag and correction factor of magnitude $1/A^2$ by Mao and Hanratty [2], where A is the ratio of magnitude of the first harmonic in $k(t)$ over that by pseudo-steady state assumption, equation (18). They are presented in Figs. 5 and 6 in accordance with the format of Mao and Hanratty [2] for easier comparison. For the case of $R = 0.1$, our numerical simulation of the full convective diffusion equation (1) are in good agreement with the solid line from analysis of linearization by Mao and Hanratty [2].

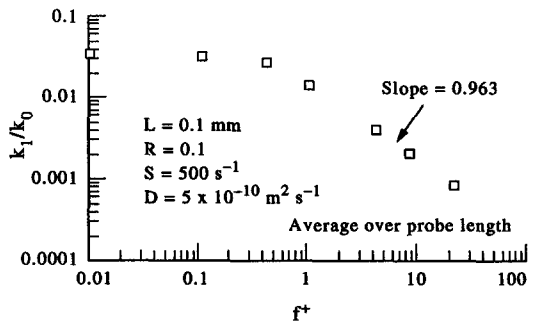

Fig. 4. Ratio of the magnitude of the first harmonic to the average of $k(t)$ vs dimensionless frequency.

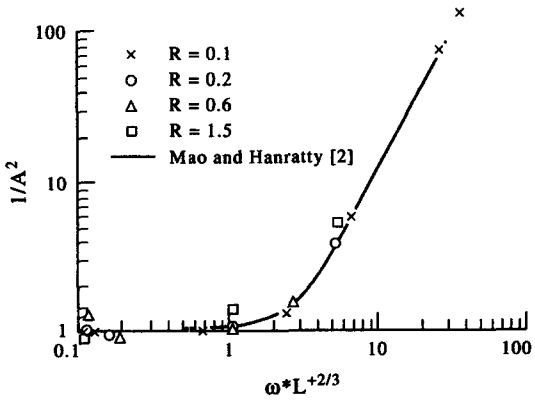

Fig. 5. Dependence of the magnitude attenuation of a single harmonic on the frequency of oscillation.

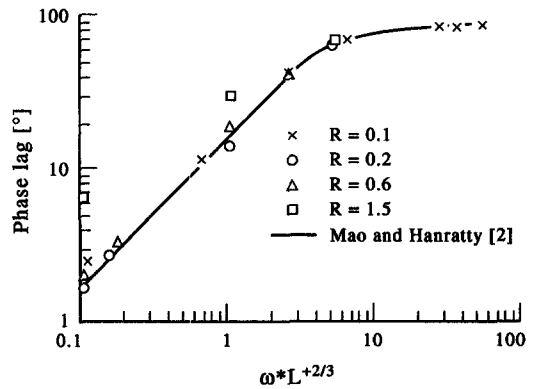

Fig. 6. Dependence of the phase lag of a single harmonic on the frequency of oscillation.

For a velocity gradient fluctuating sinusoidally with larger R, the resulting mass transfer coefficient $k(t)$ behaves quite differently. The probe response is distorted and biased from a sine wave; the phase lag becomes more obvious and unsymmetrical: the time delay is larger when S is at the minimum than that at the maximum instantaneous S, indicating the existence of higher order harmonics. More information about the influence of the fluctuation ratio R and the frequency f on the phase lag and the magnitude of the first and other higher harmonics is shown in Tables 1–4. It is noticed that the behavior of the first harmonic of k approaches the theoretical relation for steady state mass transfer, equation (18), only at low frequency and low fluctuation ratio. In Table 1, the ratio of magnitude response,

$$\psi = \frac{k_1/k_0}{(1+R)^{1/3}-1} \tag{20}$$

is tabulated. If k behaves according to $k \propto S^{1/3}$, then ψ is unity. It is noticed that frequency f and velocity gradient fluctuation R have opposite influence on ψ. Higher f suppresses the magnitude of first harmonic k_1, but high R causes an increase. These effects result from nonlinearity between C and S in equation (1) as discussed above. When the frequency is increased, every member in the family of harmonics is suppressed to some extent, the higher order harmonics being suppressed more seriously (Table 3). Table 3 also shows that the higher the frequency, the smaller is the asymmetry of $k(t)$ expressed by percentage difference of the time delay for the maximum and minimum of S due to suppressed higher harmonics. As mentioned earlier, higher frequency produces larger phase delay which approaches the asymptotic value 90° (Table 2). R is closely related to the deviation from approximation by linearization. When R is increased, the 1/3 power law is no longer valid, and larger R induces larger magnitude of all harmonic components for all frequencies tested (Table 4). Since large R will create larger amplitude of higher harmonics than the first, the asymmetry of $k(t)$ will be more serious (Table 4). Table 2 also shows that as R increases, the phase delay of the first harmonic increases too.

Table 1. Ratio of magnitude response ψ ($S_0 = 2000\ s^{-1}$, $D = 5\times10^{-10}\ m^2\ s^{-1}$, $L = 0.1$ mm)

f[Hz]	$R = 0.1$	$R = 0.2$	$R = 0.6$	$R = 1.5$
1	1.041	1.079	1.284	3.197
10	0.846	1.037	1.206	3.183

The attenuation and phase lag of the first harmonic in cases of higher value of R are also presented in Figs. 5 and 6 in comparison with Mao and Hanratty [2]. For the case of a single harmonic component in $S(t)$ and when R is small, numerical results show that the system behaves predictably in accordance with the linear relationship presented by Mao and Hanratty [2], as shown in Figs. 5 and 6. However, for higher value of R (greater than 0.2) and over the entire frequency range, a significant difference exists between these two approaches. Tables 1–4 show that no simple rules can be resorted to for prediction. It is suggested that in a case of need, the numerical simulation as presented here is necessary for evaluation of the frequency response of a heat or mass probe under consideration.

The effect of the longitudinal diffusion on the frequency response of the probe under the fluctuating wall velocity gradient was also explored. The simulation suggests that the influence is significant when the probe has small L^*. In such a case, the probe calibration should be done more carefully.

4. FLUCTUATING SHEAR STRESS WITH MULTIPLE HARMONICS

The response of the probe was computed for an input $S(t)$ from the measurements of a falling liquid film at a Reynolds number of 310 (cited from [11]). A 0.118 s interval of $S(t)$ was chosen as one period (8.47 Hz) and decomposed into a Fourier series. The first 13 pairs of Fourier coefficients were used to recon-

Table 2. Phase lag of the first harmonic of $k(t)$ behind $S(t)$ ($S_0 = 2000\ s^{-1}$, $D = 5 \times 10^{-10}\ m^2\ s^{-1}$, $L = 0.1$ mm)

f[Hz]	$R = 0.1$	$R = 0.2$	$R = 0.6$	$R = 1.5$
0.25	0.447 (4.97 ms)*			1.91 (21.2 ms)
1	1.79 (4.96 ms)	1.80 (5.00 ms)	1.98 (5.51 ms)	6.39 (17.8 ms)
10		17.5 (4.87 ms)	18.7 (5.20 ms)	29.45 (8.18 ms)
50		62.1 (3.45 ms)		66.14 (3.67 ms)

*Figures in brackets are the phase lag in ms.

Table 3. Dependence of the magnitude of harmonics in $k(t)$ on f ($S_0 = 2000\ s^{-1}$, $R = 0.2$, $D = 5 \times 10^{-10}\ m^2\ s^{-1}$, $L = 0.1$ mm)

	Relative amplitude k_i/k_0 [%]			
f[Hz]	1st harmonic	2nd harmonic	3rd harmonic	ψ
1	6.76	0.225	0.013	0.13
10	6.50	0.190	0.010	0.10
50	3.43	0.014	0.0004	0.006

Table 4. Dependence of the magnitude of harmonics in $k(t)$ on R ($S_0 = 2000\ s^{-1}$, $f = 1$ Hz, $D = 5 \times 10^{-10}\ m^2\ s^{-1}$, $L = 0.1$ mm)

	Relative amplitude k_i/k_0 [%]				
R	1st harmonic	2nd harmonic	3rd harmonic	Asymmetry of phase lag [%]	ψ
0.1	3.36	0.056	0.002	8.3	1.041
0.2	6.76	0.225	0.013	13	1.079
0.6	21.80	2.38	0.44	36	1.284
1.5	46.27	5.91	12.98	55.2	3.197

struct the input velocity gradient time trace. Thus, harmonics above 102 Hz were neglected. Figure 7 shows the relative strength of each harmonic S_i with respect to the average S_0. That signal with $f = 8.47$ Hz was fed into the computer program, and the output $k(t)$ was converted to $S(t)$ with equation (2) and then decomposed into harmonics. The ratio of k_i/k_0 over S_0 for the output $S(t)$ is plotted in Fig. 8. As the order of harmonic increases, the probe gives decreasing response for that harmonic, namely, a smaller value for ratio of k_i/k_0 over S_i/S_0 (the middle broken line in Fig. 8).

The same $S(t)$ trace was artificially stretched or compressed in the time domain so as to get input signals with the same relative spectrum S_i/S_0 but different basic frequency. They were used as input to determine the effect of basic frequency. It is observed that the lower frequency $f = 2.12$ Hz makes the output follow the velocity gradient better, while the increased frequency $f = 21.2$ Hz makes output unable to follow input $S(t)$ closely and the enhanced time delay results in more erroneous elapsing-time between the minimum and the maximum points of the output $S(t)$.

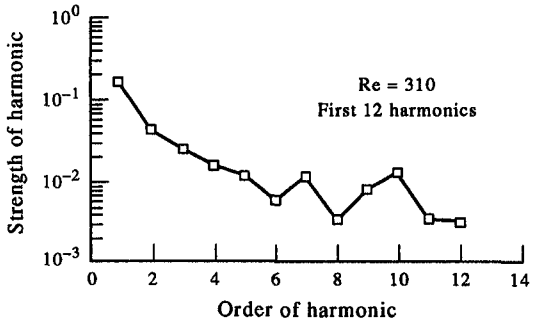

Fig. 7. Relative strength of harmonics in the input $S(t)$.

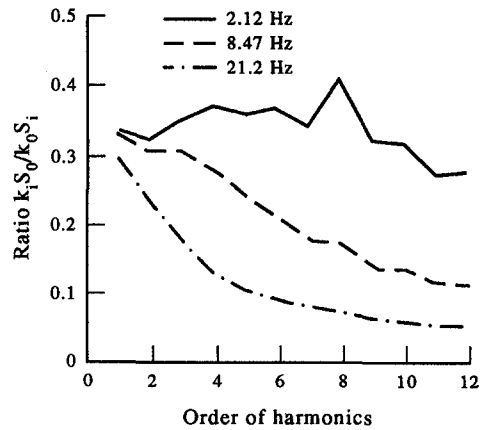

Fig. 8. Dependence of the attenuation of higher harmonics on the order of harmonics.

Figure 8 also shows that higher order harmonics in $k(t)$ for $f = 21.2$ Hz are damped more than the first few harmonics. For lower order harmonics, the ratio k_1/k_0 over S_1/S_0 is around 1/3 as the linearization theory indicated for low level of S_i, but it decays as the harmonic order increases, quite obviously for cases of $f = 8.47$ Hz and $f = 21.2$ Hz. For harmonics of the same order, the higher the basic frequency, the more serious damping results due to the high frequency for the individual component. It is noticed that a peak occurs at the 8th harmonic in Fig. 8 for $f = 2.12$ Hz, but the input $S(t)$ has no such spike at 8th order. That is additional evidence that the harmonic components are not independent of each other and a harmonic of high order in $k(t)$ is related to all the lower order harmonics in the input $S(t)$.

For the case of multiple harmonics, it can be concluded that when the input $S(t)$ has a broad spectrum in harmonic strength, the mass transfer probe produces an output $k(t)$ or $S(t)$ with a narrower spectral band with the higher order harmonics suppressed and distorted more seriously. When the dominant frequency in $S(t)$ is low, the output will conserve more original features of the input $S(t)$ and contain more information on high frequency components. Although it is not feasible to evaluate the probe behavior analytically, it is possible to use the numerical procedure to analyze the validity of using a mass transfer probe for measurements, given the information about the spectrum of $S(t)$ signal.

5. THE DOUBLE PROBE

Another case of interest is the simple oscillation of a wall velocity gradient at a double probe, which is a special situation that the wall shear stress changes its sign. A double probe is shown schematically in Fig. 1. If electrode B is downstream, then it resides in the wake of the concentration boundary layer created by electrode A and will see a thicker boundary layer as sketched in Fig. 1. Thus, if electrodes A and B have the same area of exposure, the mass transfer coefficient $k(t)$ of electrode B would be smaller than that of electrode A, indicating the direction of the flow is from A to B. When there are flow reversals at the wall, one can detect those by comparing the magnitude of the signals from a double probe. Under steady state conditions the direction of flow can be easily determined.

But oscillation of $S(t)$ around zero, in particular of high frequency, alters drastically the structure of the concentration boundary layer at a double probe. Numerical simulations were run for the input, $S(t) = 1000 \sin(2\pi ft)$, where f was chosen to be 1, 5 and 25 Hz and $D = 5 \times 10^{-10}$ m^2 s^{-1}. Figure 9(a) shows the concentration boundary layer at the moment that the velocity gradient is at its maximum value of S for three frequencies. Figure 9(a) shows that the downstream concentration boundary layer is thicker than the upstream one. For this probe L^* is small ($L^* = 14.1$) and the time constant of the probe is much less than the period of oscillation, so that the probe has enough time to follow the change of $S(t)$. With f increased to 5 Hz, upstream of the double probe there appears a large area with concentration significantly less than the bulk flow (area 'α' in Fig. 9(b)). However, the distorted boundary layer is still thicker at electrodes B than A and the direction can be determined. But the upstream concentration boundary layer has changed, and the static calibration and the single probe solution to convective diffusion equation become invalid. Further increasing f to 25 Hz brings about more change in the structure of the concentration boundary layer: it becomes more symmetric and thicker, thus resulting in a much smaller $k(t)$ (Fig. 9(c)). In this case, the period of wall shear is comparable to the time constant of the probe, and the concentration field at the probe has no sufficient time to respond to the fast oscillating velocity field and greater phase lag would result. Such systems are not suitable to determine either the direction or the magnitude of wall shear.

When measurement is made on the reversal of shear stress at the wall, it should be recognized that the probe displays greater phase lag for $S(t)$ oscillating around zero than when time-average of velocity gradient S_0 is much larger than the fluctuation. Figures 10 and 11 present the plot of attenuation defined as the ratio of k_{max} over steady state k against f^+ defined in equation (19) and the phase lag in degrees against f^+ where the data from different combinations of physical parameters fall on a unique correlation. Figure 12 shows the time trace of input $S(t) = 1000 \sin(2\pi ft)$ and resulting output $S(t)$ calculated from the difference of instant mass transfer coefficients $k_A(t)$ and $k_B(t)$,

$$k_A(t) - k_B(t) = a\left(\frac{SD^2}{L}\right)^{1/3}$$

where the constant a depends on the geometry of the double probe and the thickness of the separating insulation. When it approaches zero, a can be evaluated analytically to be 0.33 under steady state condition [6]. It is assumed that the equal voltage output from both A and B defines the moment of zero velocity gradient. Figure 12 shows that as the frequency becomes higher, severe attenuation of the maximum amplitude of $k(t)$ and rather large delay of the time of reversal picked up by a double probe with respect to the instant of zero velocity gradient. Besides, the shape of the output trace is quite distorted, suggesting serious portion of higher harmonics generated. Only at very low frequency is reasonable accuracy possible for detection of the flow reversal. Comparing the results in Figs. 10 and 11 with those in Figs. 5 and 6, it is easy to be convinced that the oscillation of shear stress around zero is the most difficult case for a mass transfer probe to respond well.

It is evident that the use of the double probe to

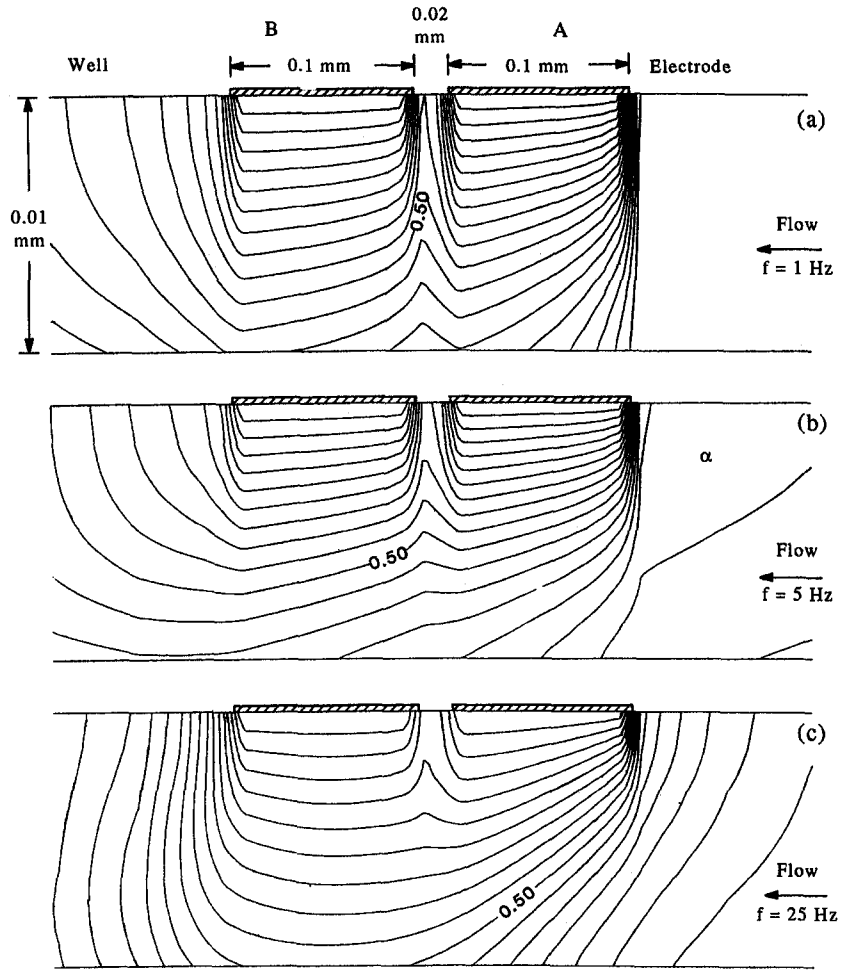

Fig. 9. Contour maps of the concentration boundary layer at a double probe when the fluctuating wall shear is at the maximum. The interval between two contour lines is 0.05.

determine direction of flow must be approached with caution. At high frequencies it seems quite useless because of the large phase shift and serious attenuation of amplitude. At lower frequencies its suitability depends on the amplitude of velocity gradient fluctuation: smaller S_{max} means larger time constant for the probe and lower frequency with which it can be used. In general, Figs. 10 and 11 supply a way to judge the suitability. If $S(t)$ is known or can be estimated, numerical simulation can be used to judge the usefulness of a double probe for the purpose.

6. CONCLUSIONS

Numerical simulation is shown to be a useful tool in designing a mass transfer probe and analyzing the

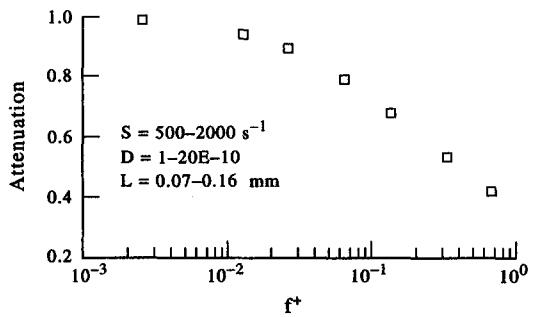

Fig. 10. Dependence of the attenuation on the dimensionless frequency.

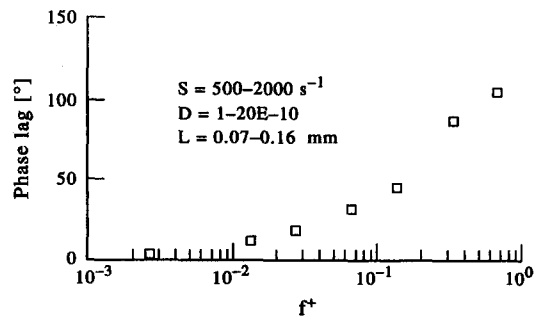

Fig. 11. Dependence of the phase lag on the dimensionless frequency.

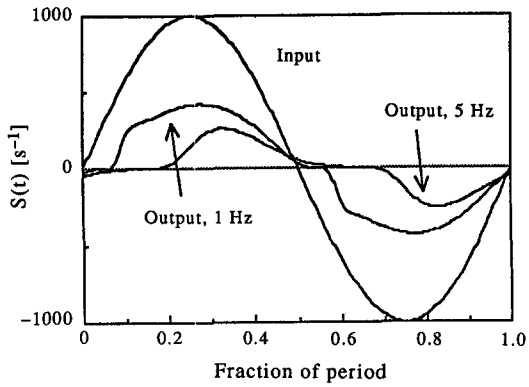

Fig. 12. Comparison of the input and output $S(t)$ by equation (2) in cases of various basic frequencies.

data from the probe. Results from the simulation confirms that the numerical procedure are suitable for the case of steady state mass transfer or a single harmonic fluctuation with a small fluctuation ratio, as presented in the literature. The numerical simulation can be used to analyze heat or mass transfer probes working in more complicated situations when analytical or linearization approaches are difficult to handle.

As pointed out above, the conventional linearization of full convective diffusion equation (1), as Fortuna and Hanratty [1] did by assuming one harmonic component in modulating velocity gradient $S(t)$ and resulting $k(t)$, is a crude idealization of physical phenomena occurring at a mass transfer probe. There is no superposition principle of $k(t)$ with respect to $S(t)$, and fluctuation of wall shear stress generates multiple harmonics in $k(t)$, even when $S(t)$ has only a simple harmonic. The harmonics in output $k(t)$ do not correspond uniquely to the same order harmonic in the input $S(t)$. The presence of strong high order harmonics in some cases makes the theory of linearization not suitable for fluctuating $S(t)$ in general.

In case of only one harmonic in $S(t)$ and the fluctuation ratio R is small, the numerical simulation gives the results in close agreement with [1] and others. Figures 5 and 6 are the comparison of numerical simulations in this study with Mao and Hanratty [2]. Despite the fluctuation of $S(t)$ up to 20%, the numerical results agree with the theory of linearization. When only one harmonic exists in the modulating flow, as typically in a laminar case, the method of correction of measurement from a mass transfer probe as suggested by Fortuna and Hanratty [1], Mao and Hanratty [2] is applicable. When R is larger than 0.2, numerical approach shows significant difference from the approximation by linearization. In this case, direct numerical simulation is suggested to evaluate any specific experimental setup.

Few real processes deal with only one harmonic. Turbulence in flow presents a significant level of higher harmonic components. The correction for measurement of shear stress reversal from a double probe is not yet resolved analytically. The mass transfer probe averages the information over the flow field and over a certain period of time of which the concentration field still keeps partial memory into a single time trace of $k(t)$. The exact recovery of the original $S(t)$ from $k(t)$ is almost impossible mathematically. Mao and Hanratty [4] have proposed a method to inverse the mass probe output. Since the longitudinal diffusion term is omitted, numerical inaccuracy will inevitably occur in the inversion, in particular when a small size electrode is used.

In summary, Figs. 5, 6, 10 and 11 set the upper limit for L for reasonable frequency response. There is no lower limit for L if an experimental calibration of S vs k is to be used. When equation (2) is used for converting $k(t)$ to $S(t)$, the lower limit for L can be determined by checking the difference between equation (2) and numerical simulation based on equation (1) with the longitudinal diffusion accounted for.

Acknowledgements—The financial support of the National Natural Science Foundation of China is gratefully acknowledged. The author is also grateful to the late Professor A. E. Dukler, University of Houston, U.S.A. for his valuable advice.

REFERENCES

1. G. Fortuna and T. J. Hanratty, Frequency response of the boundary layer on wall transfer probes, *Int. J. Heat Mass Transfer* **14**, 1499–1507 (1971).
2. Z.-X. Mao and T. J. Hanratty, The use of scalar transport probe to measure wall shear stress in a flow with imposed oscillations, *Expl Fluids* **3**, 129–135 (1985).
3. A. Ambari, C. Deslouis and B. Tribollet, Frequency response of the mass transfer rate in a modulated flow at electrochemical probes, *Int. J. Heat Mass Transfer* **29**, 35–45 (1986).
4. Z.-X. Mao and T. J. Hanratty, Application of an inverse mass transfer method to the measurement of turbulent fluctuations in the velocity gradient at the wall, *Expl Fluids* **11**, 65–73 (1991).
5. J. E. Mitchell and T. J. Hanratty, A study of turbulence at a wall using an electrochemical wall-stress meter, *J. Fluid Mech.* **26**, 199–221 (1966).
6. M. Souhar and G. Cognet, Wall shear measurements by electrochemical probe in two-phase flow—bubble and slug regimes. In *Measuring Techniques in Gas–Liquid Two-Phase Flows* (Edited by J. M. Delhaye and G. Cognet), pp. 723–744. Springer, Berlin (1984).
7. O. N. Kashinsky, Electrochemical method for studying local structure of turbulent flows. In *Near-Wall Turbulence* (Edited by S. J. Kline and N. H. Afgan), pp. 897–910. Hemisphere, New York (1990).
8. S. V. Patankar, *Numerical Heat Transfer and Fluid Flow*. Hemisphere, Washington, D.C. (1980).
9. Z.-S. Mao, An investigation of two-phase gas–liquid slug flow, Ph.D. Dissertation, University of Houston, TX, U.S.A. (1988).
10. T. Mizushina, T. Marayama, S. Ide and Y. Mizukami, Dynamic behavior of transfer coefficients in pulsating laminar tube flow, *J. Chem. Engng Jap.* **6**, 152–159 (1973).
11. G. J. Zabaras, Studies of vertical annular gas-liquid flows, Ph.D. Dissertation, University of Houston, TX, U.S.A. (1985).